Energy 342 (2026) 139646

Contents lists available at ScienceDirect

Energy

journal homepage: www.elsevier.com/locate/energy

A self-powered multiparametric sensor and valve for water distribution networks

Marco Sinagra [*], Calogero Picone, Giuseppe Lo Cicero, Daniele Puleo, Tullio Tucciarelli

University of Palermo, Engineering Department, Viale delle Scienze, Palermo, 90128, Italy

ARTICLE INFO

Handling Editor: Prof G Iglesias

Keywords:
Flow meter
Water sensor
Hydro-turbine
Hydropower
Self-powered sensors

ABSTRACT

This study presents the design, development, and experimental validation of a novel self-powered, multiparametric sensor and valve, named SWAMM, at the service of water distribution networks. The device integrates a miniaturized Cross-Flow type turbine (nano PRS type) with a built-in electrical generator, enabling energy harvesting directly from the pressurized water flow. In addition to autonomous power supply and continuous monitoring of the flow rate, SWAMM offers hydraulic regulation by means of a mobile slider mechanism. To maintain optimal turbine efficiency and reduce the volume error across variable flow rates, a flow-adaptive control strategy has been developed, supported by two polynomial functions: a quadratic law linking the flow rate with the pressure drop before the rotor, and a cubic law linking the flow rate with the head loss along the turbine. The coefficients of these functions were experimentally calibrated through laboratory testing. The SWAMM prototype was tested under controlled hydraulic conditions simulating real network operation, with flow rates ranging from 0 to 6 L/s. Results demonstrated that the device can produce up to 100 W of electrical power, with a nominal output of approximately 50 W at 2 L/s, and can operate efficiently even under partial flow conditions. Volume measurement error, assessed according to the MID European Directive, confirmed accuracy within acceptable thresholds. The harvested energy is sufficient to power also onboard electronics, communication modules (LoRaWAN), and auxiliary sensors. SWAMM sensor represents a significant advancement in smart metering, enabling both monitoring and control functions without the need of any external energy source.

1. Introduction

In recent years the increasing spread of smart technologies has radically changed the control and maintenance strategies of many civil and industrial infrastructures. More precisely, sensor technology guarantees the collection of a large amount of information related to the infrastructures and their surrounding environment. Additionally, smart sensors, endowed with energy sources, data storage units and wireless transmission, can transfer the above mentioned data to easy-to-access server units and make them available for analysis and processing.

A wide variety of applications integrated with smart sensors are today available, ranging from groundwater quality monitoring [1], to the domain of Internet of Things (IoT), where smart sensors can be employed for cyber threat detection [2]. In Water Distribution Networks (WDNs) sensor technology has been widely investigated for water pressure and quality monitoring, where chemical contamination could lead to serious public health emergencies and significant economic consequences [3]. Several studies concern the selection of the optimal number and the optimal allocation of sensors [4], also aimed to pipe burst localization based on pressure sensors through a machine learning algorithm [5]. Other researches propose installation of sensors for leakage monitoring in WDNs under uncertainty conditions, using Monte Carlo simulation to simulate leakage scenarios [6]. Different approaches were also developed for optimal allocation of pressure sensors, based on spectral clustering algorithm, used to spot WDNs areas vulnerable to leakage [7].

Most of these implementations are powered by batteries, with consequently required manual recharge. Even if in these last years the capacity of the new batteries, for given cost and size, has significantly increased, the request of new services and data type with very frequent transmission, has suggested also the use of self-powered sensors that can provide continuous monitoring without the need of external energy sources.

To this end, several applications employing energy harvesting

* Corresponding author.
E-mail addresses: marco.sinagra@unipa.it (M. Sinagra), calogero.picone@unipa.it (C. Picone), locicero.g@gmail.com (G. Lo Cicero), daniele.puleo02@unipa.it (D. Puleo), tullio.tucciarelli@unipa.it (T. Tucciarelli).

https://doi.org/10.1016/j.energy.2025.139646
Received 5 May 2025; Received in revised form 20 September 2025; Accepted 10 December 2025
Available online 11 December 2025

technologies were developed in the field of power generation through wind, solar, chemical and hydropower energies [8–10]. In hydropower generation, small hydraulic turbines, also known as microhydraulic turbines, were developed to recover unused energy in water distribution networks [11,12] and irrigation channels [13]. Pumps as turbines (PAT) were also employed to manage excessive water head reduction [14]. Recently, self-powered sensors were designed for turbine flowmeters to measure water flowrate [10] and also volumetric flowrate of the gas-liquid two-phase flow in industrial facilities such as reactors and heat-exchangers [15].

However, the electric power generated by most of these applications is only sufficient to supply the energy required by the sensor and by the data transmission, but is not large enough to control the monitored quantity via mechanic movements of the hosting device. For example, it is not possible to control the flow rate measured by the flow meter by means of a single device.

We propose here a new self-powered device embedding flow rate measurement and control, for water distribution networks. The new device, developed in the context of the SWAMM (Smart Water Metering and Management) project, is given by a nano PRS cross-flow turbine with a special regulation mobile component, named slider. The primary objective of the proposed device is to integrate flow measurement and flow control functionalities within a single, electrically self-powered unit.

The device can either maximize the energy production and measure the flow rate with a small and limited head dissipation (passive mode), approximately 5 m of water column, typical of volumetric water meters, or control the flow rate with a higher head dissipation (active mode). The produced mean power, in the test case of a flow meter serving about 40 habitants, is about 100 W, which is much larger than the required one, even in the case of frequent active modes. This allows to use the proposed device also as energy provider of other sensors; including pressure, temperature, turbidity and other quality parameters.

The paper is organized as follows: in section 2 a brief presentation of the PRS turbine and its design criterium is provided; in section 3 the single electric and mechanic components of the device, along with the slider design and control, are described; in section 4 a SWAMM sensor prototype is described. Experimental results are shown and discussed in section 5; conclusions follow in section 6.

2. Background: PRS type turbine

Cross-flow (CF) turbines are popular action turbines working in the same head-flow range of the Francis ones. In spite of a bit smaller efficiency, CF turbines are much cheaper, mainly because of the cylindric shape of the internal and external blade surface. Recently, a reaction type version of the CF turbine, named Power Recovery System (PRS) has been proposed by the authors [16,17] to be used for low-head and/or inline installation along aqueducts. See, in Fig. 1, a sketch of the PRS section normal to the axis.

A major issue, to get a good energy production from the PRS turbine, is its capability to maintain high efficiencies with different flow rates. For this purpose, a specific mobile device has been recently designed and tested [19]. The device is a slider aimed to control the surface A of the inlet flow cross-section according to the actual flow rate, when this flow rate becomes smaller than the design one (see Fig. 2). This allows to keep the inlet velocity of the runner constant and the velocity ratio Vr close to its optimal value 2, without changing the rotational velocity. Vr is defined as:

$$V_r = \frac{V \cos \alpha}{\omega R} \tag{1}$$

where V is the norm of the velocity at the rotor inlet surface, α is the angle of the velocity vector with respect to the tangent to the same surface, ω is the rotational velocity and R is the rotor radius.

The main parameters of the PRS turbine, i.e the radius of the rotor and its length can be computed by solving, along with Eq. (1), the following equations in the V, R and W_{max} unknowns:

$$Q_{max} = V \sin \alpha \;\; R \;\; \lambda W_{max} \tag{2}$$

$$V = C_V \sqrt{2g\left(\Delta H - \xi \frac{\omega^2 R^2}{2g}\right)} \tag{3}$$

where Q_{max} is the maximum flow rate of the turbine, λ is the runner inlet angle, C_v is a non-dimensional coefficient equal to 0.98, g is the gravitational acceleration, ΔH is head jump and ξ is a non-dimensional coefficient equal to 1 in the case of free outlet flow or equal to 2.1 in the case of pressurized outflow. More information about the PRS design can be found in Refs. [16–18].

3. A self-powered multiparametric sensor and valve

Multiparametric sensors offer numerous advantages for monitoring water networks. Continuous measurement of pressure and water flow at various points in the network, along with other parameters such as pH, turbidity, conductivity, and temperature, can provide a comprehensive real-time overview of the water service quality, as well as a rapid identification of anomalies or critical events. More precisely, the SWAMM sensor has been designed to measure pressure and flow rate, while extracting for self-powering a small amount of hydraulic energy from the pipe where it is installed. It is based on the Venturi effect occurring in the converging channel between the section of the hosting pipe and the first section of the nozzle of the microturbine (Fig. 2). The resulting differential pressure Δp is directly related to the flow rate and its range is guaranteed, even for small discharges, through the regulation

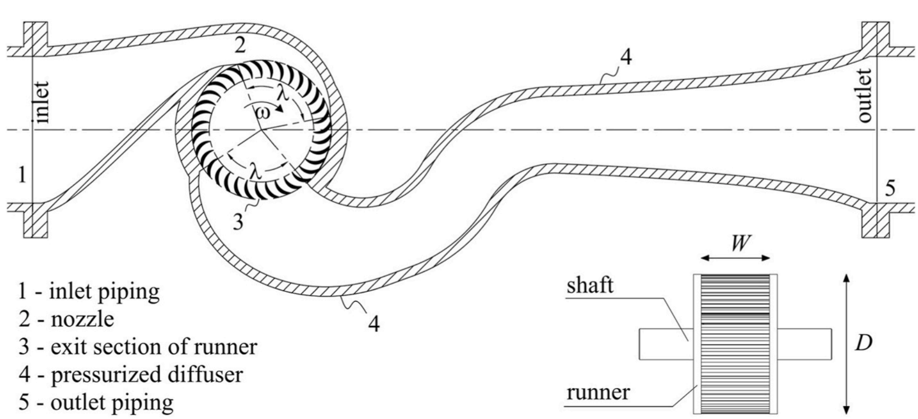

Fig. 1. Section of a PRS turbine.

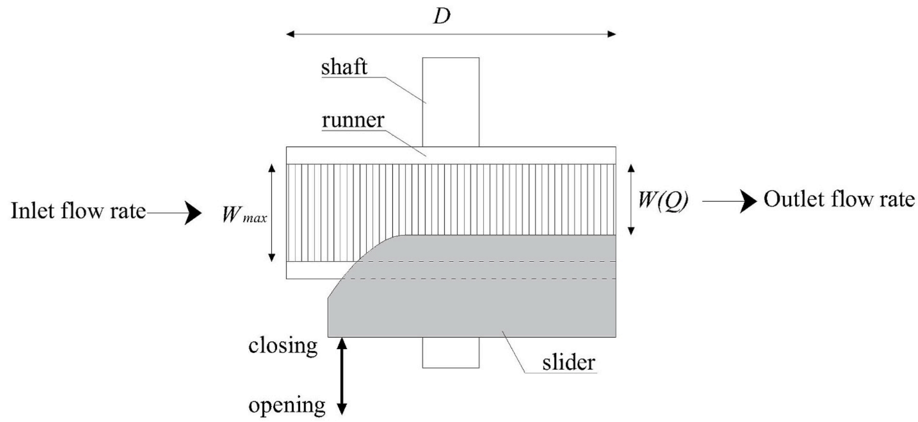

Fig. 2. PRS regulation system.

of a mobile slider, controlling the distance between the two walls of the nozzle orthogonal to the runner axis (Fig. 2). The energy produced by the generator charges a buffer battery, which powers the regulation system, the onboard electronics (including components needed for remote communication), and additional sensors - such as those for pressure and water quality - that can be easily integrated in the device.

If the SWAMM sensor is switched from ‘passive‘ to ‘active’ mode, the same slider can be used to limit the flow rate delivered to the water user by means of remote control.

3.1. SWAMM sensor components

One of the functionalities of the SWAMM sensor is to generate electric power by means of a PRS turbine. This turbine, like all traditional hydraulic turbines, follows a typical scheme in which two machines – the hydraulic turbine and the electric generator – are mechanically connected through their respective drive shafts. This arrangement allows the hydraulic runner, which is immersed in the pressurized fluid, to operate while the generator remains in an atmospheric environment. For this purpose, the hydraulic turbine always incorporates a hydraulic seal that enables the transition of the turbine shaft between the two different environments (Fig. 3).

In the case of low-power turbines, and high pressure hosting pipe, the use of hydraulic seals provides a significant dissipative loss [19], due to the sliding between the fixed and the rotating components. To eliminate these losses, the hydroelectric configuration of the SWAMM sensor integrates the generator within the hydraulic runner, merging both in the pressurized fluid environment, thereby eliminating the need of hydraulic seals. More precisely, the geometries of both the stator and the rotor of the hydraulic turbine are designed according to traditional PRS criteria. For the generator section of the device, a brushless configuration with rotating permanent magnets has been selected. In this configuration, a rotating cylindrical case, with the same rotor diameter, is added on one side of it (Fig. 4) to provide support for a ferromagnetic cylinder equipped with the generator’s permanent magnets. The central part of the resulting cylinder is occupied by the stator of the electric generator, which consists of a ferromagnetic core wound with copper windings and the associated electronics. The entire electric stator is attached to the turbine case, with the only connection to the unpressurized external environment being made by the electrical cables using a static hydraulic seal. With this configuration, the entire generator is immersed in water and electrically isolated from it by a dedicated layer of epoxy resin. Fig. 4 shows the structure of the hydraulic runner – electric generator assembly of the SWAMM sensor.

The main installation point of the SWAMM sensor is the inlet pipe serving a small community of 30–40 people. At this location, it is well known that flow rates undergo significant variations, depending on the demand of the served users. In order to maximize the electrical power generation efficiency of the turbine, and to maintain a constant velocity ratio as shown in Equation (1), the SWAMM sensor is also equipped with a slider (Fig. 5), aimed to control the width W of the flow cross-section immediately before the inlet of the hydraulic runner. The slider is actuated by a stepper motor, in order to ensure accurate control of its movement. The device configuration is completed with a differential pressure transducer, which measures the water pressure difference between the sensor’s inlet section and the section corresponding to the variable narrowing defined by the slider (Fig. 5). Given the slider position and the differential pressure measurement, the SWAMM sensor computes the instantaneous water flow rate using the algorithm described in the following section, based on the Venturi effect in converging pipes.

The power provided by the generator is used for five main functions:

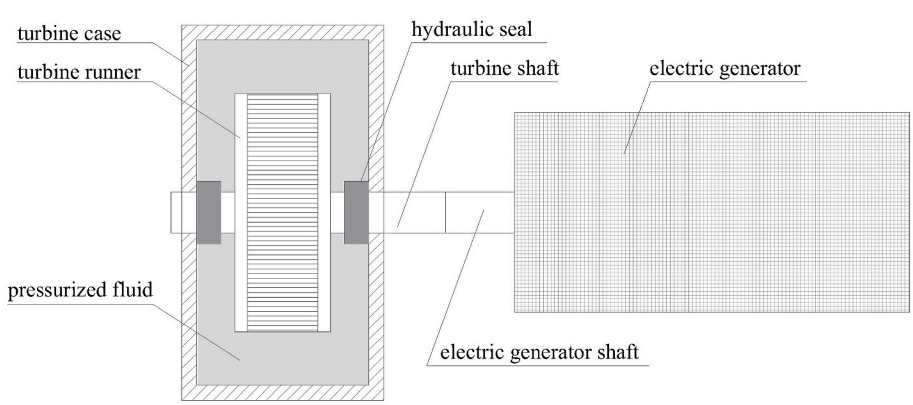

Fig. 3. Typical scheme of hydropower turbine.

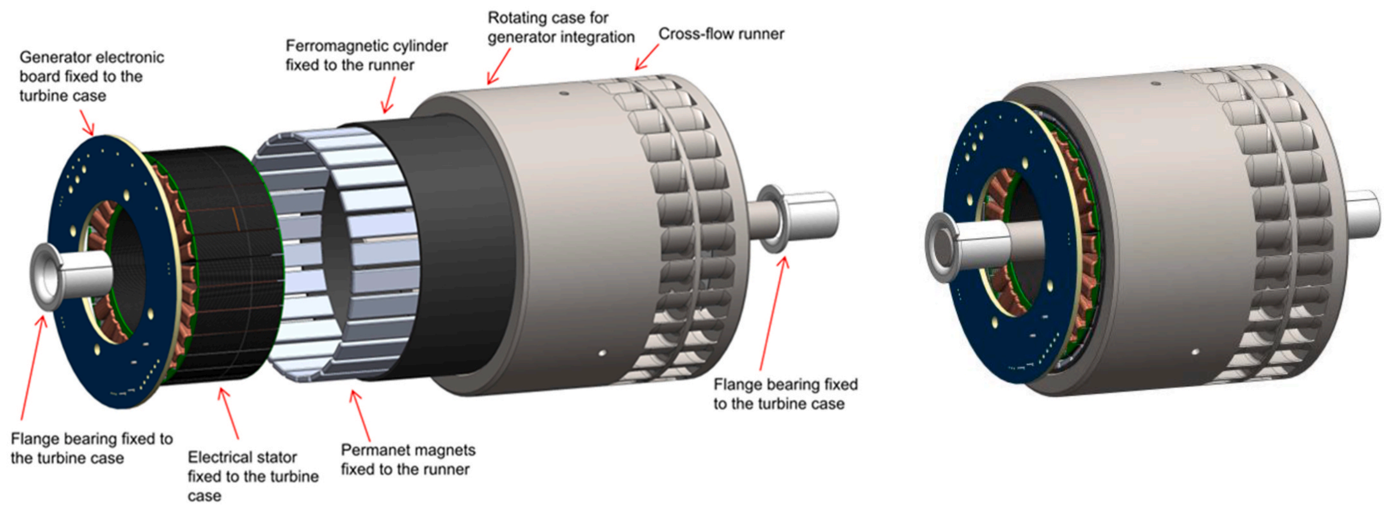

Fig. 4. SWAMM sensor rotor components (exploded view in the left, assembled view in the right).

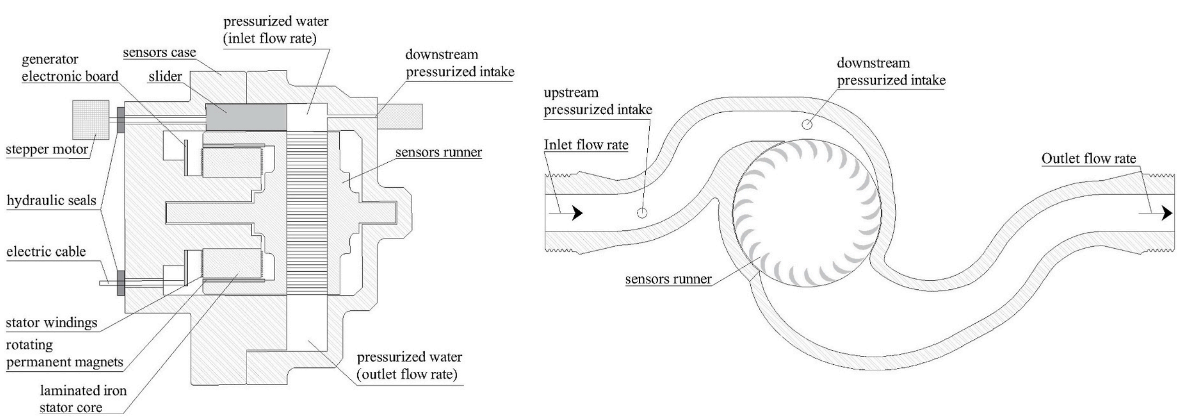

Fig. 5. SWAMM sensor components (cross section on the left; longitudinal section on the right).

1) battery recharging; 2) regulation of the runner's rotational speed to the design value; 3) stepper motor powering for slider actuation; 4) supplying internal devices; 5) supplying any external device. Function 1) is achieved through a current-controlled battery charger, with the aim of guaranteeing the availability of electrical energy in the event of low or zero water flow; Function 2) is implemented by dissipating part of the generated power in a ballast electric load using a Pulse Width Modulation (PWM) system controlled by a Proportional–Integral–Derivative (PID) algorithm.

3.2. Data transmission and remote control

The SWAMM sensor is connected to the LoRaWAN system and managed through the ChirpStack server. The adopted LoRaWAN system allows the SWAMM sensor to transmit consumption data every 5 s, as well as to receive commands for slider actuation. ChirpStack is an open-source LoRaWAN network server which enables safe management of flow data between the meter and the application in both directions, while offering flexible integration with third-party systems. ChirpStack supports multi-tenant configurations, encrypted data transmission, and scalable deployment, making it a robust and cost-effective solution for smart utility management. Data collection, processing, and visualization by authorized users are enabled through the SWAMM application server, which features a backend developed in Kotlin Spring language.

3.3. Flow meter algorithm and slider control logic

The proposed SWAMM sensor calculates the flow rate by assuming a quadratic relationship between the pressure drop Δp measured by the differential manometer, for a fixed position of the slider, and the water flow rate Q, as expressed in Equation (4):

$$\Delta p = a_{(i)} Q^2 + b_{(i)} Q \tag{4}$$

where $a(i)$ and $b(i)$ are coefficients which depend on the *i-th* position of the slider. It should be observed that the pressure variation Δp is measured between two points located upstream of the turbine runner, and that Equation (4) is independent of the runners's rotational speed.

In order to maximize the electrical power generation, the slider position can be optimized on the basis of the instantaneous flow rate in order to get an hydraulic jump ΔH, between the inlet and outlet turbine sections, as close as possible to the design one ΔH_{opt}. It should be observed that the ΔH_{opt} value can be remotely adjusted according to the operating conditions of the aqueduct, for example during exceptional events in which it is mandatory to limit the pressure reduction downstream of the device. We assume the following cubic relationship to hold between the hydraulic jump ΔH and the flow rate Q:

$$\Delta H = c_{(i)} Q^3 + d_{(i)} Q^2 + e_{(i)} Q \tag{5}$$

where $c(i)$, $d(i)$ and $e(i)$ are coefficients which depend on the *i-th* position of the slider.

The coefficients of Equations (4) and (5) are obtained through experimental calibration tests of the sensor.

The algorithm applied to compute the flow rate and the slider position involves the following steps, as shown in the flowchart of Fig. 6.

1) Instrumental acquisition of the differential pressure Δp;
2) Instrumental acquisition of the slider position s;
3) Flow rate Q calculation using Equation (4);
4) Estimation of the hydraulic jump ΔH;
5) Slider position s* updating, if the squared difference between ΔH and ΔH_{opt} is too large.

Concurrently with the cyclic flow rate estimation and slider positioning algorithm, the rotational speed of the runner is actively controlled. The control process begins by validating a runner rotation velocity strictly greater than zero. If this condition is satisfied, the rotational speed is regulated to match the design value by adjusting the electrical load on the generator. This is achieved either via the battery charging system or, in the case of a fully charged battery, through the dissipation of excess power in electrical resistive loads.

With respect to the data transmission time interval described in Section 3.2, the processing described here is performed by the onboard electronics, which estimates the flow rate every 100 ms and performs the remaining operations at intervals of 5 ms.

4. SWAMM sensor prototype

To evaluate the performance of the proposed sensor, a prototype of the SWAMM device was designed and constructed. The design of the prototype followed the methodology outlined in the previous section, with a nominal flow rate of 2.5 L/s and a design hydraulic head ΔH_{opt} of

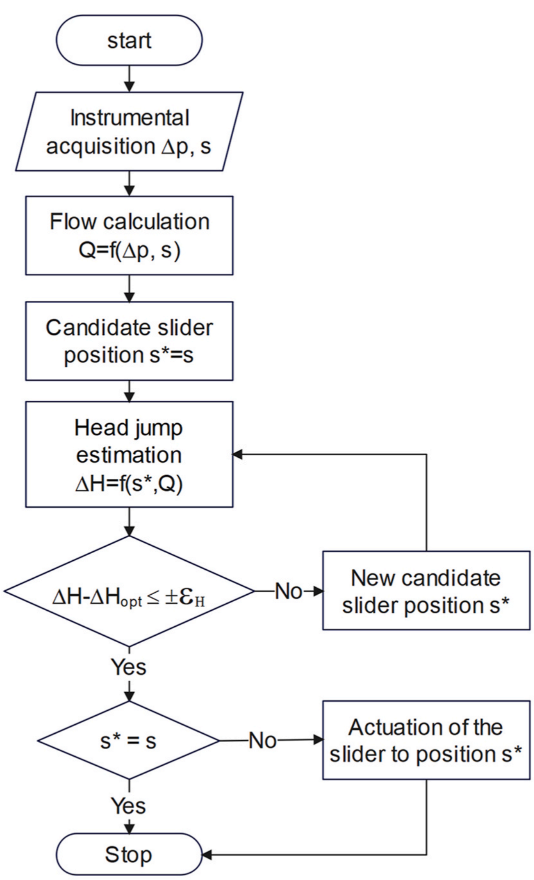

Fig. 6. Flowchart of the flow rate estimation and slider positioning algorithm.

6 m of water column. On the basis of a runner rotational speed of 1000 RPM, the rotor diameter and width were set equal to 80 mm and 20 mm, respectively. The rotor was manufactured with stainless steel and equipped with 28 blades. The slider component was made of bronze, and the sensor housing was also constructed with stainless steel. The overall length of the prototype is 340 mm, which is consistent with that of commercial flow meters designed for comparable flow rates (Fig. 7).

The device includes a brushless three phase electric generator with rotating magnets and static electric windings. The runner is a single body with the bell containing the magnets. The stator is encapsulated in epoxy resin and is fully immersed in water (Fig. 8). This solution minimizes the gap between the magnets and the ferromagnetic teeth of the stator, increasing the efficiency and the power of the generator. The water contributes to the dissipation of the heat produced inside the stator. The configuration of the generator is with 28 high energy NeFeB magnets (Figs. 8) and 24 ferromagnetic teeth with the electric windings. The stator also includes three magnetic Hall sensors, a temperature sensor and other auxiliary electronic components. The generator can also be used as a motor, for diagnostic purposes.

Before the hydraulic tests, the electrical generator alone was characterized using an external motor as the drive system. Power generation tests were conducted at different rotational speeds and varying electrical loads. The resulting power curves are presented in Fig. 9. It can be observed that, at the sensor's design speed, the electrical power output reached 100 W. The generator characterization at a constant speed of 1000 RPM demonstrated an almost constant efficiency, exceeding 90 % within the expected load range for the SWAMM sensor, as shown in Fig. 10.

5. Experimental results

The hydraulic characterization of the SWAMM prototype was performed using a custom-built test bench. The bench consists of a closed-loop system featuring a 1.5 m^3 storage tank and a 5.5 kW multistage centrifugal pump. The main loop pipeline has a diameter of 2 inches (50.8 mm), a total length of 5 m, and includes a bypass line measuring 1.2 m in length with a diameter of 0.5 inches. The bench is equipped with pressure transducers and electromagnetic flow meters installed on both the main and bypass lines, allowing for accurate measurement of low flow rates through the bypass. The setup enables the simulation of operating conditions with flow rates ranging from 0 to 6 L/s and upstream pressures up to 8 bar. A photo of the test bench is shown in Fig. 11.

5.1. Prototype characterization

Before performing the measures of the water volume, a second order polynomial regression has been carried out for 20 different slider positions i, between a large number of differential pressure Δp and corresponding flow rate measures Q, estimated with the two master flow meters (Fig. 12). These tests enabled the calibration of the coefficients $a(i)$ and $b(i)$ in Eq. (4). The resulting coefficients are reported in Table 1. Observe that, under normal operating conditions, the rotational velocity of the rotor may fall below 1000 RPM, depending on the instantaneous available hydraulic power. If the available hydraulic power is sufficient to drive the rotor at a higher speed, the electrical load (e.g., battery charging systems or braking resistors) will be activated to limit the rotational velocity to the design value.Nevertheless, the obtained results show that the coefficients are independent of the rotor's rotational velocity. This behaviour is explained by the specific placement of the two pressure measurement points, both located upstream of the runner (Fig. 5).

The head difference ΔH, between the sensor's inlet and outlet, was also measured as function of the flow rate. These measurements were used to calibrate the coefficients $c(i)$, $d(i)$ and $e(i)$ in Equation (5) (Table 2). See in Fig. 13 the characteristic ΔH-Q curves of the sensors,

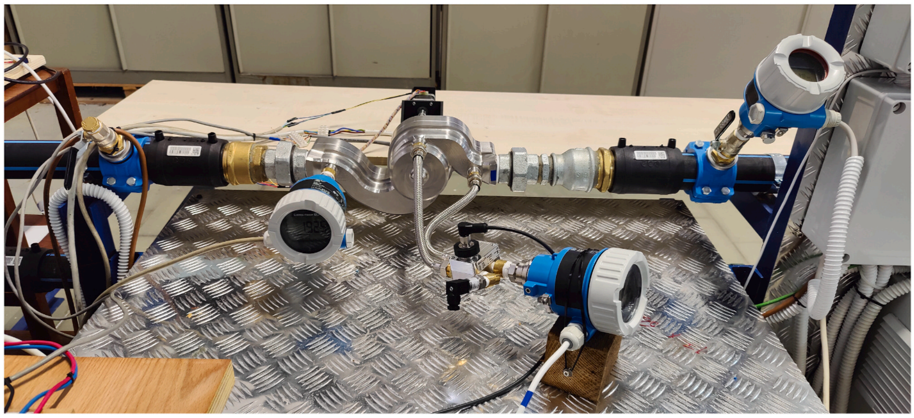

Fig. 7. SWAMM sensor prototype installed in the main line of the experimental bench.

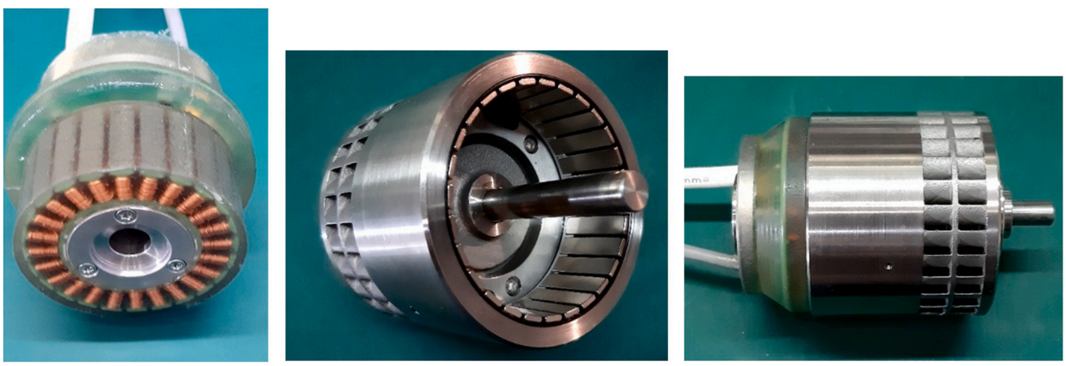

Fig. 8. SWAMM sensor electric generator (a: electric stator encapsulated in epoxy resin; b: electric rotor; c: assembly of hydraulic runner and electrical generator).

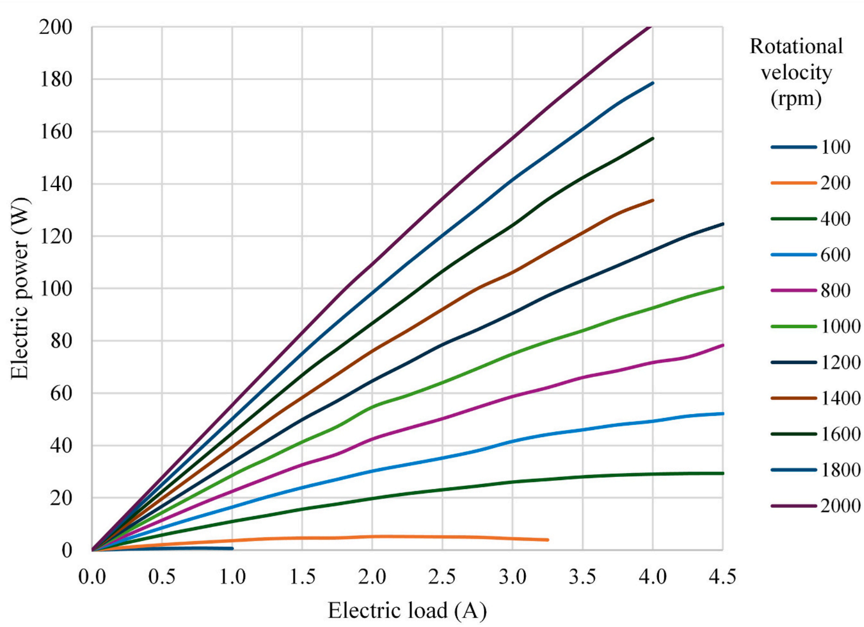

Fig. 9. Electric power versus electric load of the SWAMM electric generator.

each one for a different slider position. Observe that ΔH was measured only for calibration of the sensor coefficients. In field applications, a second pressure transducer downstream of the SWAMM rotor is not required.

5.2. Prototype volume error estimation

The SWAMM prototype volume error has been estimated by comparison with certified master meters, i.e. Hendress & Hauser DMA20-AAAAA1, in the by-pass line for flow rates smaller than 0.4 l/s and

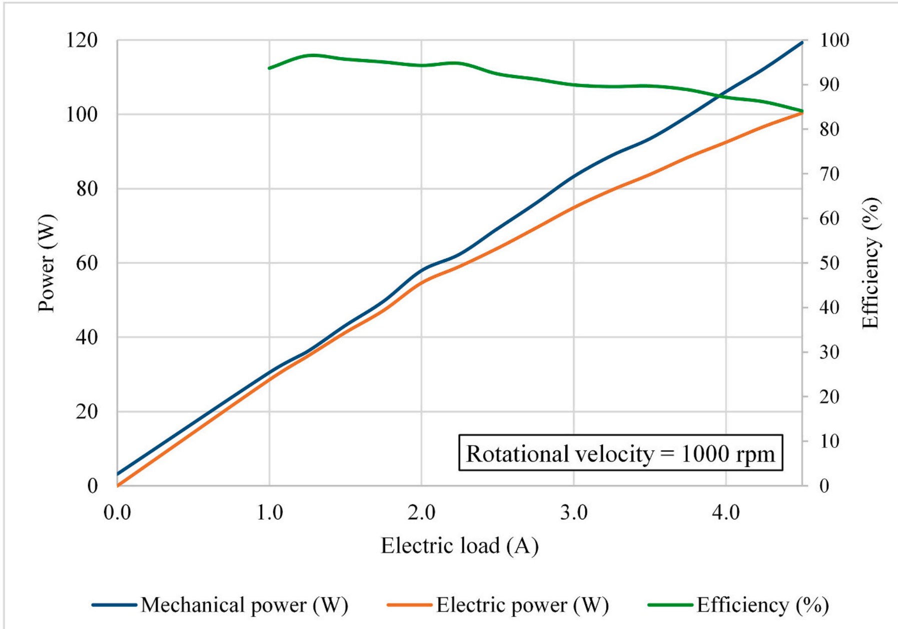

Fig. 10. Mechanical power and Electric power versus electric load of the SWAMM electric generator.

Fig. 11. Experimental facility overview.

Hendress & Hauser DMA50-AAAAA1, in the main line for flow rates greater than 0.4 l/s.

According to the European Directive 2014/32/UE MID (Measuring Instruments Directive), the volume estimation error must be evaluated at four characteristic flow rates of the water meter: the minimum value Q_1, the permanent design flow rate Q_3, the transient flow rate Q_2 between Q_1 and Q_3, the maximum flow rate Q_4. For the SWAMM sensor, the four characteristic flow rates and the corresponding flow rate errors are reported in Table 3.

The residual error in the volume estimation within the device is mainly due to the measurement uncertainty of the pressure and position sensors, as well as to the typical signal fluctuations under the unsteady hydrodynamic conditions in which the device operates.

5.3. Electrical power production

Under nominal operating conditions, the generated electrical power is approximately 50 W and can exceed 100 W at higher water flow rates. For a constant nominal flow rate of 2 L/s, the corresponding daily energy production is approximately 1.2 kWh. In the case of typical domestic water usage, the estimated average generated power is around 2.5 W, which corresponds to approximately 60 Wh per day.Even under worst-case conditions, the generated energy is sufficient to reliably power the internal components of the device, as well as some external sensors and low-power actuators. In scenarios with higher average flow rates, it becomes possible to supply energy to higher-power external devices as well.

6. Conclusion

A fully integrated self-powered sensor for water distribution networks has been successfully developed and tested. The SWAMM device combines a flow-adaptive hydraulic turbine and a multiparametric sensing system, capable of measuring and regulating flow rate while generating electrical power from the hydraulic energy of the network. The prototype demonstrated robust performance under varying hydraulic conditions, delivering up to 100 W of electrical power—well above the requirements of its internal systems and additional low-power

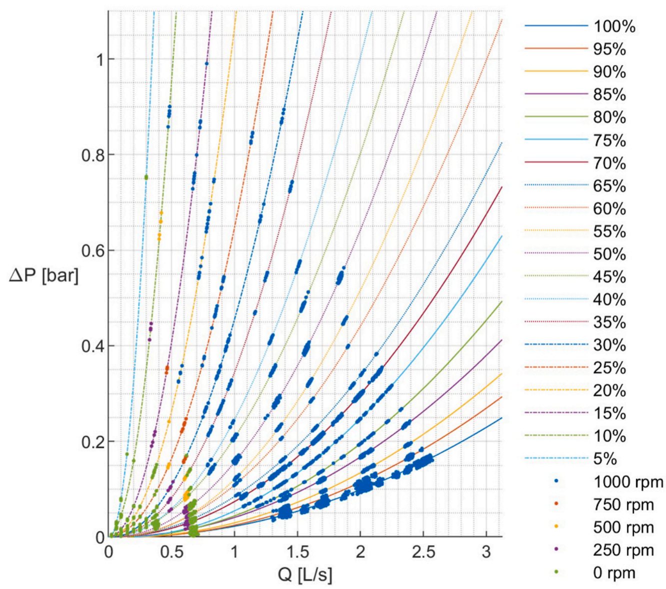

Fig. 12. Experimental points and range estimation curves of the SWAMM sensor.

Table 1
Equation (4) coefficients.

Slider opening (*i*) [%]	*a(i)*	*b(i)*	Slider opening (*i*) [%]	*a(i)*	*b(i)*
5	8.60770	−0.07776	55	0.13789	−0.01759
10	3.69200	0.07162	60	0.11198	−0.00347
15	1.63840	−0.00704	65	0.08466	−0.00020
20	1.08540	−0.01911	70	0.07563	−0.00179
25	0.63858	0.00789	75	0.06930	−0.01488
30	0.47536	−0.02085	80	0.05362	−0.00971
35	0.36110	−0.01717	85	0.04299	−0.00237
40	0.25708	−0.01174	90	0.03773	−0.00836
45	0.19384	0.01373	95	0.03272	−0.00832
50	0.16248	−0.00490	100	0.02713	−0.00494

sensors or actuators. The accuracy in volume measurement was assessed in accordance with the European MID Directive. The results show that the SWAMM sensor satisfies the MID requirements for most characteristic flow rates, with only minor deviations observed in the lowest flow rate range, where measurement uncertainty is inherently higher. The system's independence from external power sources, combined with remote communication capabilities via LoRaWAN, highlights its potential for large-scale deployment in smart water networks. The proposed device not only improves operational efficiency and monitoring resolution but also contributes to energy recovery and sustainability goals in water infrastructure.

Future work will focus on field validation of the sensor, with particular attention to its energy generation performance and data transmission reliability. This will allow a detailed analysis of the device's energy storage capabilities and an accurate quantification of the daily energy consumption of the onboard electronics and actuation system.

CRediT authorship contribution statement

Marco Sinagra: Writing – review & editing, Writing – original draft, Validation, Supervision, Methodology, Formal analysis, Conceptualization. **Calogero Picone:** Writing – original draft, Software, Investigation, Data curation. **Giuseppe Lo Cicero:** Writing – original draft, Software, Investigation, Conceptualization. **Daniele Puleo:** Writing – original draft, Investigation. **Tullio Tucciarelli:** Writing – original draft, Supervision, Project administration, Methodology, Funding acquisition, Conceptualization.

Funding

Open access funding provided by Università degli Studi di Palermo within the CRUI-CARE Agreement. This work was supported by the

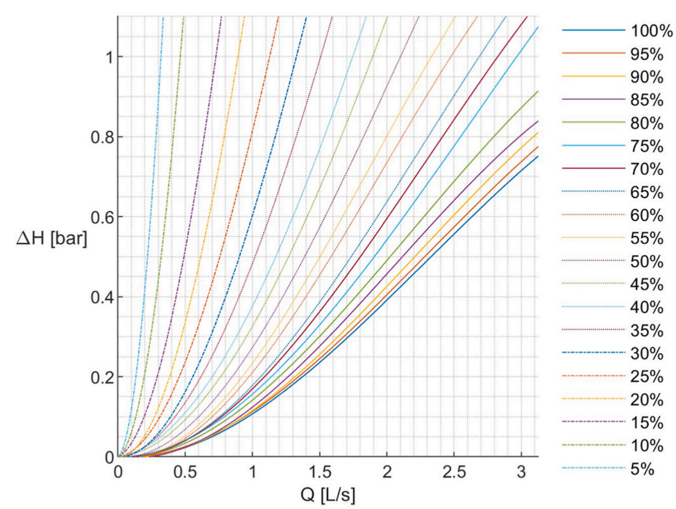

Fig. 13. *ΔH* curves versus flow rate of the SWAMM sensor.

Table 3
Characteristic flow rates and measurement errors of the SWAMM sensor.

Flow rate	Flow rate ratio	Tested values	Estimated volume error
Q_1	$Q_3/40$	0.0625 L/s	4.26 %
Q_2	$Q_3/25$	0.1 L/s	2.96 %
Q_3	Q_3	2.5 L/s	1.82 %
Q_4	1.25 x Q_3	3.125 L/s	−0.41 %

Table 2
Equation (5) coefficients.

Slider opening (*i*) [%]	*c(i)*	*d(i)*	*e(i)*	Slider opening (*i*) [%]	*c(i)*	*d(i)*	*e(i)*
5	−2.61680	9.95150	0.20320	55	−0.06132	0.35092	−0.05599
10	−1.57180	5.22550	0.10137	60	−0.05443	0.32014	−0.05511
15	−0.37914	1.93150	0.16470	65	−0.03691	0.25125	−0.03635
20	−0.31340	1.55230	−0.02035	70	−0.03282	0.22677	−0.02468
25	−0.18149	0.94685	0.04738	75	−0.02355	0.18533	−0.00540
30	−0.11635	0.73031	−0.01135	80	−0.02914	0.19124	−0.02067
35	−0.07036	0.52943	0.02410	85	−0.03244	0.20188	−0.04560
40	−0.03854	0.36719	0.04802	90	−0.02648	0.17710	−0.03544
45	−0.04119	0.34544	0.02182	95	−0.02297	0.15837	−0.02251
50	−0.05568	0.35667	−0.02775	100	−0.02298	0.15752	−0.02745

project "SWAMM - Azione 1.1.1 POC 2014–2020 Completamento graduatoria Azione 1.1.5 P.O. FESR SICILIA 2014–2020 Cod. Prog 08CT00CT270264 CUP G77H18001660006″

Declaration of competing interest

The authors declare that they have no known competing financial interests or personal relationships that could have appeared to influence the work reported in this paper.

Data availability

Data will be made available on request.

References

[1] Venkatesh J, Partheeban P, Baskaran A, Krishnan D, Sridhar M. Wireless sensor network technology and geospatial technology for groundwater quality monitoring. Journal of Industrial Information Integration 2024;38:100569. https://doi.org/10.1016/j.jii.2024.100569.

[2] Pundir S, Wazid M, Singh DP, Das AK, Rodrigues JJPC, Park Y. Intrusion detection protocols in wireless sensor networks integrated to internet of things deployment: survey and future challenges. IEEE Access 2019;8:3343–63. https://doi.org/10.1109/access.2019.2962829.

[3] Palleti VR. Optimal sensor placement for contamination detection and identification in water distribution networks under demand uncertainty. Comput Chem Eng 2025:109003. https://doi.org/10.1016/j.compchemeng.2025.109003.

[4] Najarzadegan MR, Moeini R. Maximizing the coverage of quality sensors in the water distribution network (case studies: Lee and Deininger and the second and the third EPANET networks). Results Eng 2025:104334. https://doi.org/10.1016/j.rineng.2025.104334.

[5] Lo Presti J, Giudicianni C, Toffanin C, Creaco E, Magni L, Galuppini G. Combining clustering and regularised neural network for burst detection and localization and flow/pressure sensor placement in water distribution networks. J Water Process Eng 2024;63:105473. https://doi.org/10.1016/j.jwpe.2024.105473.

[6] Tornyeviadzi HM, Owusu-Ansah E, Mohammed H, Seidu R. Node search space reduction for optimal placement of pressure sensors in water distribution networks for leakage detection. Alex Eng J 2024;94:325–38. https://doi.org/10.1016/j.aej.2024.03.037.

[7] Bezerra D, Giudicianni C, Creaco E, Meirelles G, Brentan B. A novel approach based on graph signal processing and sampling theory to set pressure sensors in water distribution networks. Expert Syst Appl 2025:126306. https://doi.org/10.1016/j.eswa.2024.126306.

[8] Rao CK, Sahoo SK, Yanine FF. An internet of things–based intelligent smart energy monitoring system for solar photovoltaic applications. Elsevier eBooks; 2024. p. 375–416. https://doi.org/10.1016/b978-0-443-13392-3.00019-0.

[9] Duan Z, Yuan Z, Jiang Y, Zhao Q, Huang Q, Zhang Y, Liu B, Tai H. Power generation humidity sensor based on primary battery structure. Chem Eng J 2022;446:136910. https://doi.org/10.1016/j.cej.2022.136910.

[10] Uchiyama T, Takamure K, Okuno Y, Sato E. Development of a self-powered wireless sensor node to measure the water flowrate by using a turbine flowmeter. Internet of Things 2021;13:100327. https://doi.org/10.1016/j.iot.2020.100327.

[11] McNabola A, Coughlan P, Corcoran L, Power C, Williams AP, Harris I, Gallagher J, Styles D. Energy recovery in the water industry using micro-hydropower: an opportunity to improve sustainability. Water Policy 2014;16:168–83. https://doi.org/10.2166/wp.2013.164.

[12] Du J, Ge Z, Wu H, Shi X, Yuan F, Yu W, Wang D, Yang X. Study on the effects of runner geometric parameters on the performance of micro Francis turbines used in water supply system of high-rise buildings. Energy 2022;256:124616. https://doi.org/10.1016/j.energy.2022.124616.

[13] Satou E, Uchiyama T, Takamure K, Ikeda T, Okayama T, Miyazawa T, Tsunashima D. Changes in power generation performance of an undershot cross-flow-type hydraulic turbine in an irrigation channel due to snow masses passing through the rotor. Heliyon 2023;9:e20833. https://doi.org/10.1016/j.heliyon.2023.e20833.

[14] Du J, Yang H, Shen Z, Chen J. Micro hydro power generation from water supply system in high rise buildings using pump as turbines. Energy 2017;137:431–40. https://doi.org/10.1016/j.energy.2017.03.023.

[15] Uchiyama T, Miyamoto S, Horie K, Takamure K. Simultaneous measurement of volumetric flowrates of gas–liquid bubbly flow using a turbine flowmeter. Sensors 2023;23:4270. https://doi.org/10.3390/s23094270.

[16] Sinagra M, Sammartano V, Morreale G, Tucciarelli T. A new device for pressure control and energy recovery in water distribution networks. Water (Switzerland) 2017;9:5. https://doi.org/10.3390/w9050309.

[17] Sinagra M, Picone C, Aricò C, Pantano A, Tucciarelli T, Hannachi M, Driss Z. Impeller optimization in crossflow hydraulic turbines. Water (Switzerland) 2021;13:3. https://doi.org/10.3390/w13030313.

[18] Picone C, Sinagra M, Aricò C, Tucciarelli T. Numerical analysis of a new cross-flow type hydraulic turbine for high head and low flow rate. Eng Appl Comput Fluid Mech 2021;15(1):1491–507. https://doi.org/10.1080/19942060.2021.1974559.

[19] Picone C, Sinagra M, Tucciarelli T. A new regulation system for crossflow type turbines for water management industry. Energy 2025;328. https://doi.org/10.1016/j.energy.2025.136695.